energies

MDPI

Article

A Study of a Two-Phase Heat Transfer Mechanism in a Vertical Sintering Cooling Furnace

Weihui Xu [1], Qinbao Wang [1], Juan Zhen [1,2], Weishu Wang [1,*], Yan Peng [3], Boyan Tian [1], Yushuai Ruan [1] and Renjie Li [1]

[1] College of Energy and Power Engineering, North China University of Water Resources and Electric Power, Zhengzhou 450045, China; xuweihui@ncwu.edu.cn (W.X.); z202210050619@stu.ncwu.edu.cn (Q.W.); zhenjuan@stu.ncwu.edu.cn (J.Z.); tianby2019@163.com (B.T.); ysruan@163.com (Y.R.); lrj1501491780@outlook.com (R.L.)
[2] Cscec Scimee Sci.& Tech. Co., Ltd., Chengdu 610045, China
[3] Citic Heavy Industries Co., Ltd., Louyang 471039, China; 13938871853@163.com
* Correspondence: wangweishu@ncwu.edu.cn

Abstract: In order to explore the law of gas–solid countercurrent cooling heat transfer in a vertical sinter cooling furnace at a high temperature, based on the Euler model and the local non-thermodynamic equilibrium theory, an exergy efficiency model was built to evaluate the heat transfer process in the vertical sinter cooling furnace with different parameter changes. It was found that the inlet temperature of cooling air and sinter inlet temperature are the main factors affecting the temperature field and gas–solid heat transfer characteristics in the furnace. Under the conditions of each parameter, the cooling air temperature presents a radial "M" shape distribution. The axial cooling section is the most intense area of gas–solid heat transfer, and this part has the best heat transfer effect. When the inlet temperature of cooling air and the inlet temperature of sinter increase, the outlet temperature of sinter and the outlet temperature of cooling air increase. When the sinter equivalent diameter increases, the cooling air outlet temperature decreases gradually, while the sinter outlet temperature increases gradually. When the diameter and height of the cooling section increase, respectively, the outlet temperature of the sinter decreases and the outlet temperature of the cooling air increases. Based on dimensional analysis, the heat transfer correlation formula suitable for certain test conditions is obtained.

Keywords: high-temperature sintered ore vertical cooling furnace; gas–solid counterflow cooling heat transfer; exergy efficiency model; heat transfer correlation

Citation: Xu, W.; Wang, Q.; Zhen, J.; Wang, W.; Peng, Y.; Tian, B.; Ruan, Y.; Li, R. A Study of a Two-Phase Heat Transfer Mechanism in a Vertical Sintering Cooling Furnace. *Energies* **2024**, *17*, 761. https://doi.org/10.3390/en17030761

Academic Editor: Dmitry Eskin

Received: 11 November 2023
Revised: 10 December 2023
Accepted: 13 December 2023
Published: 5 February 2024

1. Introduction

The iron and steel industry is an important basic industry in China, but it has a long process and high energy consumption, with an energy efficiency of only 30–50%. The sintering process, which is the third most energy-consuming process, has a waste heat recovery rate of only 22%, with more than 70% of the waste heat not being utilised. Efficient recycling of sintering waste heat is of great significance to the steel industry in terms of energy saving, consumption reduction, quality improvement and efficiency enhancement [1]. The traditional cooling methods are ring cooling and belt cooling; the disadvantages of these methods include poor containment, uneven cooling of the sintered ore, and low waste heat recovery [2]. A vertical sintering cooling furnace is formed based on dry coke quenching technology, which has the advantages of low air leakage rate, high waste heat recovery rate, etc. [3].

The gas flow and gas–solid heat transfer problems inside the vertical cooling furnace of sinter ore are the key problems affecting the waste heat recovery of vertical cooling furnace. Feng Junsheng's team established an unsteady gas–solid heat transfer model in the ring cooler and analysed the influence of different parameters on the waste heat recovery of

the ring cooler [4]. Based on the porous medium model and combined with the gas–solid packing bed dynamics theory, a mathematical model of gas flow in the sintered vertical tank was established [5]. According to the regression analysis of the experimental data, the modified Ergun correlation and gas–solid heat transfer correlation are obtained [6]. The gas–solid heat transfer characteristics of sinter were studied by establishing an experimental device for gas–solid heat transfer [7]. The basic law of gas–solid heat transfer process in vertical tank of sinter waste heat recovery was studied in combination with experiment and numerical simulation [8]. The air pressure drop performance in the sinter bed was studied experimentally, and the correlation of air FPD in the sinter BL was described in the form of Eu [9]. TIAN et al. [10] established a numerical calculation model of three-dimensional flow and heat transfer in the ring cooler, optimized and analysed the operating parameters of the ring cooler, and established a model with the exergic heat recovery as an objective function [11]. Tian Fuyou et al. [12] studied the influence of wall effect in vertical cooling furnace on the resistance coefficient, and proposed the resistance prediction formula of mixed particle size sinter filled bed [13]. In order to accurately analyse the gas resistance in a packed bed with different particle sizes, many scholars have revised the Ergun equation from the perspectives of wall effect [14,15], particle shape [16] and particle size distribution [17,18]. Soma [19] and Dunbar et al. [20] were the first to propose the concept of exergy transmission. Zude Cheng et al. [21] conducted detailed energy efficiency and exergy efficiency analyses on gas–solid heat transfer in vertical coolers. Prommas et al. [22] investigated the effect of porous structural parameters and thermodynamic conditions on the energy and exergy transfer process. Acevedo et al. [23] analysed the heat loss and irreversible properties of a holding furnace based on the first and second laws of thermodynamics.

The above literature illustrates that the vertical furnace cooling process is an important means of recovering steel waste heat with high efficiency, and the introduction of the exergy can better evaluate the effectiveness of the process, but the related research is relatively lacking at present. In order to obtain the law of gas–solid countercurrent heat transfer in a vertical sinter ore cooling furnace, the key technology of coordinated matching of furnace cooling gas–solid flow field is developed to achieve continuous, stable and efficient cooling in a high-temperature sinter ore furnace. A simulation study of the cooling furnace structural parameters and operating parameters on the vertical sinter ore furnace system gas–solid countercurrent heat transfer law, revealing the high temperature sintered ore cooling heat transfer law, obtained the heat transfer correlation that can be used in certain test conditions, providing the theoretical basis for the development of subsequent vertical sinter ore cooling furnace.

2. Modelling of Vertical Cooling Furnaces

Numerical simulation is used to analyse the vertical cooling furnace. This section describes the mathematical model, physical model, mesh model, and boundary conditions used in the simulation.

2.1. Mathematical Mode

2.1.1. Continuity Equation

$$\frac{\partial(\varepsilon\rho)}{\partial t} + u\frac{\partial(\varepsilon\rho u)}{\partial x} + v\frac{\partial(\varepsilon\rho v)}{\partial y} + w\frac{\partial(\varepsilon\rho w)}{\partial z} = 0 \quad (1)$$

where ε is the porosity of sintered ore; ρ is the air density, kg/m^3; u, v, and w are the velocity components of the air in the x, y, and z directions, respectively, m/s.

2.1.2. Equation of Motion

$$\frac{\partial}{\partial x_j}(u_i u_j) = \left[\frac{\partial}{\partial x_j}\left(\mu\frac{\partial u_i}{\partial x_j}\right) - \frac{\partial P}{\partial x_j} + \frac{\partial}{\partial x_j}\left(\mu\frac{\partial u_j}{\partial x_i}\right) - \frac{2}{3}\frac{\partial}{\partial x_i}\left(\mu\frac{\partial u_j}{\partial x_j}\right)\right] + g_i - f_i + S_i \quad (2)$$

where u_i is the apparent velocity of air in the direction i, m/s; u_j is the apparent velocity of air in the direction j, m/s; g_i is the volume force of air in the direction of i, f_i is the resistance acting in the opposite direction per unit volume of air, N/m^3; P is the surface force of air, N/m^2; S_i is the source term in the direction of i, N/m^3.

2.1.3. Equation for Conservation of Energy

The fluid energy equation is:

$$\varepsilon(\rho c)_f \frac{\partial T_f}{\partial \tau} + (pc)_f u_f \cdot \nabla T_f = \varepsilon\nabla \cdot \left(\lambda_f \nabla T_f\right) + \varepsilon q_f + h_v\left(T_s - T_f\right) \quad (3)$$

The solid energy equation is:

$$(1-\varepsilon)(\rho c)_s \frac{\partial T_s}{\partial \tau} = (1-\varepsilon)\nabla \cdot (\lambda_s \nabla T_s) + (1-\varepsilon)q_s - h_v\left(T_s - T_f\right) \quad (4)$$

where ρ_f is the air density, kg/m^3; ρ_s is the density of ore, kg/m^3; T_f is the temperature of cooling air, K; T_s is the temperature of sintered ore, K; h_v is the integrated volumetric heat transfer coefficient, $W/(m^3 \cdot K)$.

2.1.4. Equations for Exergy and Exergy Efficiency

"Exergy" is the usable energy, which represents the maximum amount of energy that can be reversibly converted into useful work to the maximum extent possible in theory. Exergy can be used as a parameter to evaluate the value of energy. Since the pressure inside the vertical cooling furnace is not much different from the ambient pressure, the value of exergy carried by the cooling air is calculated by the temperature of the cooling air, and the expression is as follows:

$$e_{f,out} = (h_{f,out} - h_0)(1 - \frac{T_0}{T_{f,out} - T_0} \ln \frac{T_{f,out}}{T_0}) \quad (5)$$

The exergy-value of the outlet cooling air per unit time:

$$E_{f,out} = e_{f,out} \cdot q_f \quad (6)$$

From Equations (5) and (6):

$$E_{f,out} = (h_{f,out} - h_0)(1 - \frac{T_0}{T_{f,out} - T_0} \ln \frac{T_{f,out}}{T_0}) q_f \quad (7)$$

Similarly, the value of exergy of the inlet cooling air per unit time is known as:

$$E_{f,in} = (h_{f,in} - h_0)(1 - \frac{T_0}{T_{f,in} - T_0} \ln \frac{T_{f,out}}{T_0}) q_f \quad (8)$$

The sintered ore carries a value of exergy per unit time:

$$E_{s,in} = (h_{s,in} - h_0)(1 - \frac{T_0}{T_{s,in} - T_0} \ln \frac{T_{s,out}}{T_0}) q_s \quad (9)$$

where T_0 is the ambient temperature and is taken as 273.15 K; $T_{f,out}$ is the cooling air outlet temperature, $T_{f,in}$ is the cooling air inlet temperature, $T_{s,in}$ is the sintered ore inlet temperature, $T_{s,out}$ is the sinter outlet temperature K; h_0 is the enthalpy of cooling air at ambient state, $h_{f,out}$ is the enthalpy of cooling air at inlet temperature, and $h_{s,in}$ is the enthalpy of sintered ore at inlet temperature, kJ/kg.

Energy in the process of conversion will have the problem of energy loss, exergy efficiency can succinctly and effectively represent the effect of waste heat recovery in the cooling process; the expression is as follows:

$$\eta_e = \frac{E_{f,out} - E_{f,in}}{E_{s,in}} \tag{10}$$

2.2. Geometric Model

In the vertical sinter ore cooling furnace, the cooling air is sent into the cross-shaped duct by the air supply device, and after passing through the cross-shaped duct, the air is sent to the furnace by the air cap. And when heat exchange is completed, the high temperature gas enters into the waste heat boiler from the outlet to generate electricity. The geometrical model of the vertical sinter cooling furnace is shown in Figure 1, where (**a**) is the schematic diagram of the three-dimensional structure of the vertical sinter ore cooling device, and (**b**) is the sectional view at the central axis of the sinter ore cooling device. H is the height of the cooling section, D is the diameter of the cooling section, and α is the tilting angle of the air cap.

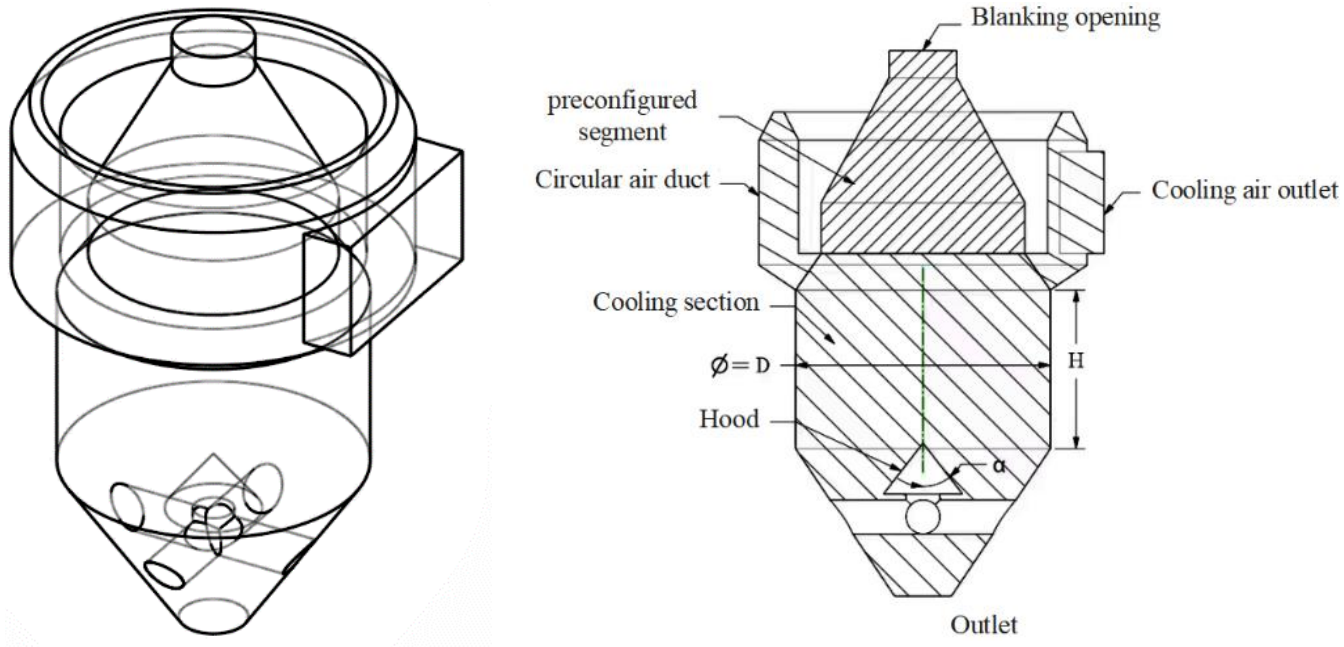

Figure 1. Schematic diagram of geometric structure of vertical sinter cooling furnace. (**a**) Three-dimensional schematic of the model; (**b**) schematic of the profile of the model.

2.3. Mesh Model

Unstructured meshing is carried out in the computational region of the model using Fluent 2020 R2, and the appropriate mesh size is selected to ensure the computational speed and achieve the computational accuracy at the same time. As the tip of the cone is prone to mesh distortion, the local mesh of the air cap part is encrypted. Figure 2 is a schematic diagram of the grid model.

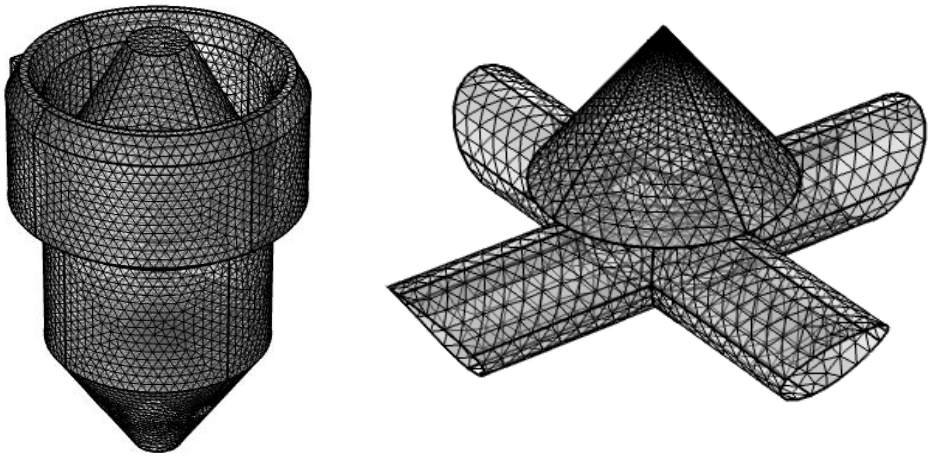

(**a**) (**b**)

Figure 2. Grid model diagram of vertical sinter cooling device. (**a**) Integral mesh model; (**b**) local hood mesh model.

The calculated results are affected by the number and quality of model meshes, and the mesh model is verified for independence before numerical calculation. Specific working conditions are selected for mesh independence validation, and the specific parameters are shown in Table 1.

Table 1. Table of calculated working parameters.

Parameters	Numerical Value
Mass flow rate of sintered ore (kg/s)	102
Inlet speed of cooling air (m/s)	7.8
Inlet temperature of sintered ore (°C)	750
Inlet temperature of cooling air (°C)	20
Sintered ore particle diameter (mm)	14.25
Cooling section diameter (m)	9.0
Height of cooling section (m)	6.0

Variations in sinter outlet temperature and cooling air pressure loss are selected to verify the independence of the grid model, and five different numbers of grid models are obtained based on the number and quality of grids, and the results are shown in Figure 3. Grid 4 is selected for the simulation with a grid number of 1.46 million.

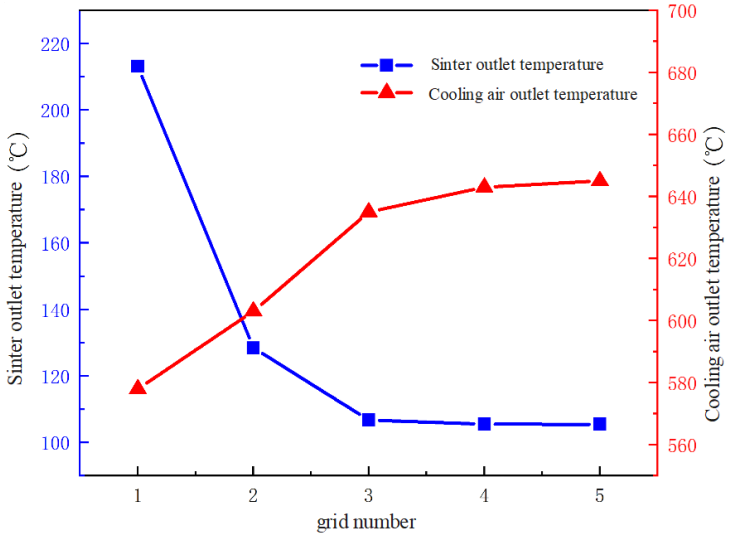

Figure 3. Mesh irrelevance verification.

2.4. Model Reliability Verification

The vertical cooling process for sinter ore is not yet commonly used in existing industrial practice, and the paper chose to compare the accuracy of the heat transfer calculation model with the experimental data from the literature [24]. The working condition parameters are as follows: gas velocities of 0.4 m/s, 0.8 m/s, 1.2 m/s, 1.6 m/s, 2.0 m/s, particle equivalent diameter of 11.45 mm, and height of the cooling section of 0.455 m. The gas flow resistance per unit height/L under the above working condition parameters is compared and analysed in terms of the trend of gas flow resistance per unit height with respect to the inlet velocity of the cooling air. The results of a comparative analysis of the simulated and measured values are shown in Figure 4, the error is within 10%, in line with the requirements of model validation.

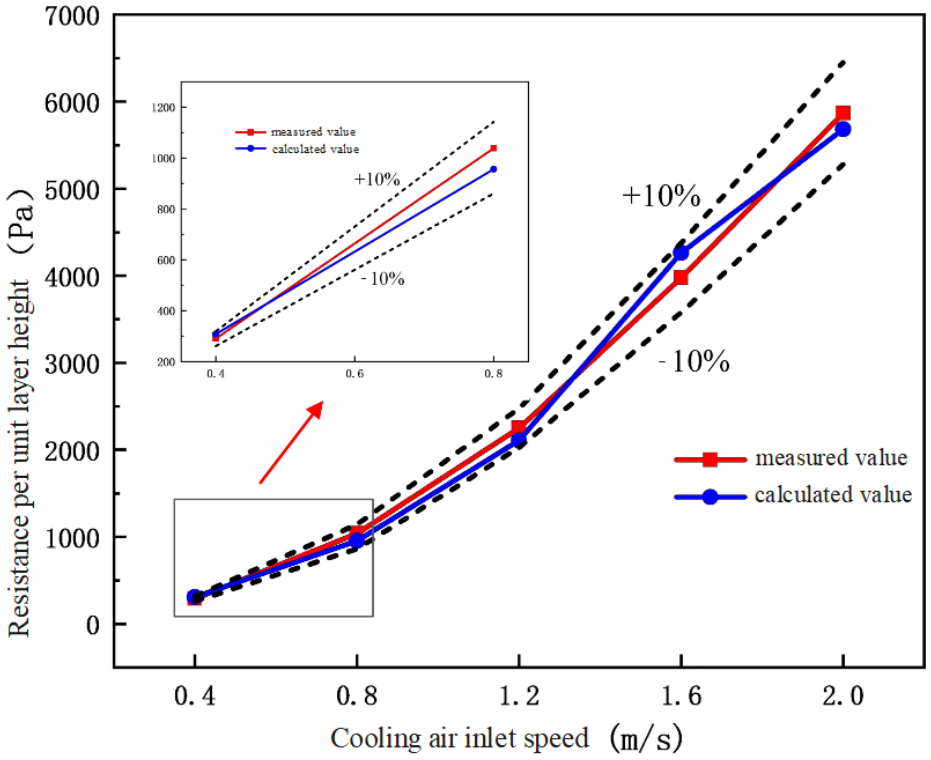

Figure 4. Comparison of measured and calculated values of resistance per unit of material layer under different working conditions.

2.5. Boundary Conditions

A sinter cooling furnace is a typical gas–solid heat transfer device, and the gas–solid two-phase heat transfer process in the cooling furnace is very complicated. If various factors in reality are taken into account, the calculation will be too complicated and difficult, and it is difficult to achieve accurate mathematical modelling and simulation research. The shape of the sinter ore in actual production is irregular, and the size of the ore particle is very uneven, so it is difficult to conduct an accurate numerical description and simulation research on it. At the same time, the particle size of the ore is very small relative to the diameter of the cooling furnace, so the sinter ore in the furnace can be averaged and statistically processed. Therefore, under the condition of ensuring the accuracy of the simulation calculation and reflecting the law of gas–solid heat transfer and flow, the problem of flow heat transfer in cooling furnace is simplified.

The boundary conditions in the simulation involve thermal and flow variables. Considering that the flow of cooling wind in the furnace is incompressible, the boundary conditions were set as follows: (1) the cooling air flow inside the duct is not considered, and the conical surface on the air cap is used as the inlet condition for the cooling air velocity; (2) the cooling air outlet is a pressure outlet; (3) the sintered ore inlet flow size

is set to 102 kg/s, and the outlet at its bottom is a pressure outlet; (4) the wall surface is adiabatic; inside the cooling furnace body; and (5) there is only sintered ore, so the portion of the mesh except for the annular air ducts is defined as the porous medium zone, and the porous zone is homogenised.

3. Influence of Gas–Solid Heat Transfer in Vertical Cooling Furnaces

The main parameters that affect the heat transfer effect of vertical sinter cooling furnace include operating parameters and structural parameters. The operating parameters mainly include cooling air inlet temperature, sinter inlet air temperature equivalent diameter, and the structural parameters include cooling section height and cooling section diameter.

3.1. Effect of Cooling Air Inlet Temperature on Gas–Solid Heat Transfer Characteristics

The heat transfer process in the furnace was numerically simulated by changing only the inlet air temperature. The inlet air temperature parameters are shown in Table 2, in which the inlet temperature is 750 °C, the height of the cooling section is 7 m, the diameter of the cooling section is 11.25 m, and the equivalent diameter of the sinter is 14.45 mm.

Table 2. Simulation parameters for inlet air temperature.

serial number	1	2	3	4	5	6
Inlet air temperature (°C)	20	30	40	50	60	70

In order to obtain the effect of sinter equivalent diameter on the temperature field in the furnace, it is necessary to analyse the axial and radial temperature distribution of the cooling air in the furnace with the equivalent diameter.

The central section of sinter vertical cooling furnace is selected as the characteristic section to reflect the change in axial cooling air temperature in the furnace. The z = 3.5 m section is the characteristic section, which reflects the change in radial cooling air temperature in the furnace.

As can be seen from Figure 5, the temperature of the cooling air in the central section of the furnace gradually becomes larger when the inlet temperature of the cooling air becomes larger. This is due to the fact that with the increase in the inlet air temperature, when other parameters in the furnace remain unchanged, the heat exchange effect between the cooling air and the hot sintered ore is enhanced, so that the temperature of the cooling air also increases. In addition, the temperature of the cooling air is lower in the furnace near the wall and at the hood. This is due to the high flow rate of the cooling air at the hood and the shorter heat exchange time with the hot sinter, so the temperature of the cooling air at this place is lower compared with that in the centre of the furnace. As the sintered ore particles near the wall are larger, and there are more gaps between the particles, which is conducive to the flow of cooling air, the contact area between the cooling air and the sintered ore is larger, and the heat exchange effect is stronger, so the temperature of the cooling air in this area is also lower.

Figure 6 shows that the cooling air temperatures show a trend of higher temperatures in the centre part than in the surroundings in all this cross-section, and with the increase in the inlet air temperature, the temperature of the cooling air in this cross-section also increases. The main reason is that the sintered ore in the centre part of the furnace is more closely stacked, and the sintered ore particles in this part are smaller and at higher temperatures, while the smaller gaps between the particles of this part of the sintered ore lead to a higher cooling air velocity in this part, and the heat exchange between the cooling air and the sintered ore is stronger in this region, and the temperature of the cooling air is also higher. In addition, with the increase in inlet air temperature and the constant flow rate of cooling air inlet, the apparent flow rate of gas in the furnace increases. This phenomenon makes the time required for the sinter at the same temperature inlet to be cooled to a certain temperature decrease continuously. When the sinter moves at a certain speed, the contact

time between the cooling wind and the sinter increases, so the temperature of the cooling wind also increases successively.

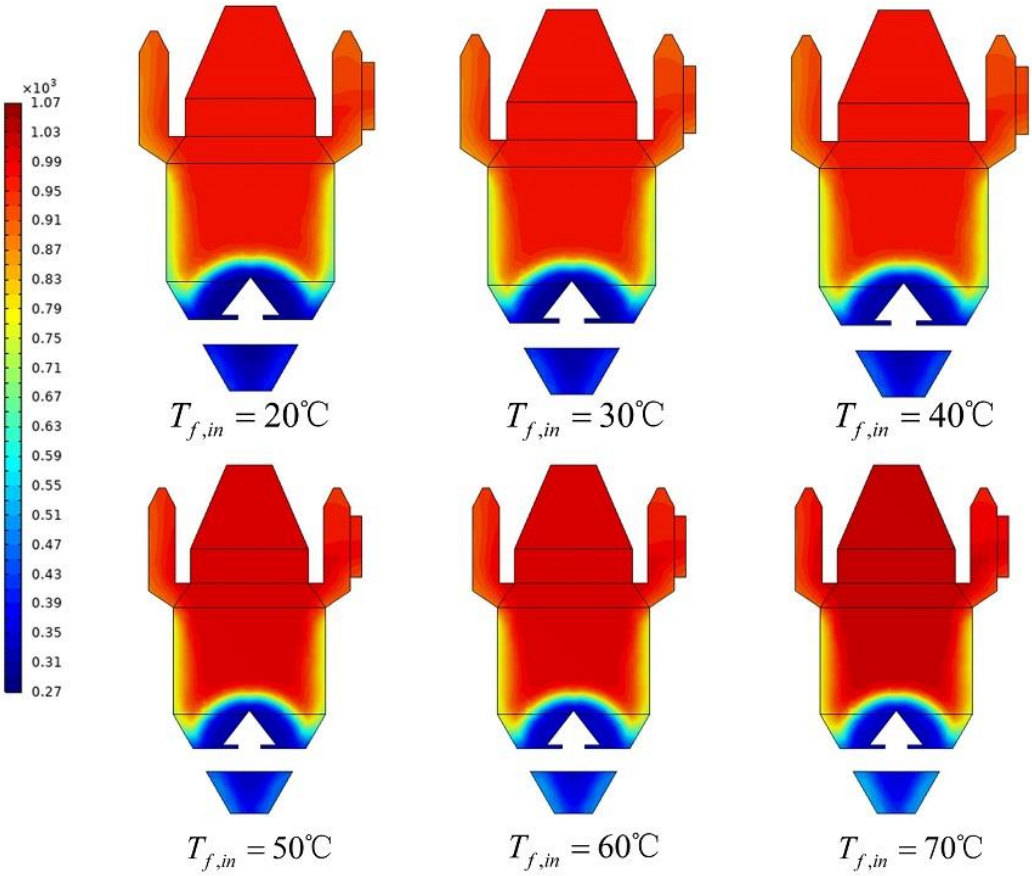

Figure 5. Variation in cooling air temperature with cooling air inlet temperature at the central section of the furnace.

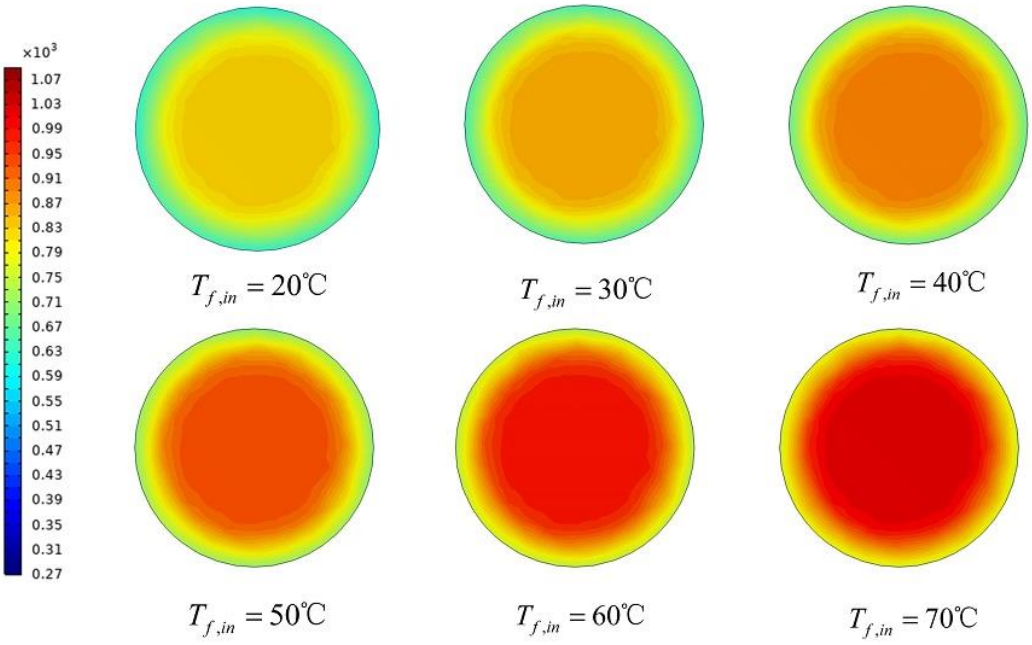

Figure 6. Variation in cooling air temperature with cooling air inlet temperature.

A radial straight line is taken for a certain height in the furnace to reflect the variation law of each parameter of the section at the same height in the furnace. In order to clearly observe the changes of the section at the same height and select the section with drastic parameter changes for analysis, the line graph with z = 1 (the radial direction is taken at 1 m above the hood) is selected for data processing.

Figure 7 shows the variation in cooling air temperature along the axial direction at different cooling air inlet temperatures. As can be seen from Figure 5, the temperature of the cooling air in the pre-storage section under different cooling air inlet temperature is basically unchanged, because in the pre-storage section of the cooling air flow is extremely slow, this part of the basic is not involved in the heat transfer, so the temperature of the cooling air in the pre-storage section of the basic remains unchanged in each operating condition. In the main cooling section from −2 m to 2 m, the heat exchange between the sinter and the cooling air is the most intense, and the heat exchange effect of this part is greatly affected by the inlet air temperature. As the inlet air temperature increases, the temperature difference between the cooling air and the sinter decreases, and the heat exchange efficiency decreases. Therefore, when the inlet air temperature of the cooling air rises, the temperature of the cooling air in the furnace is also higher. The section from 2 m to 7 m is the secondary heat exchange area, and the temperature of sintered ore in this area is higher. With the increase in inlet wind temperature, the heat exchange effect between sintered ore and cooling wind becomes weaker, the heat exchange coefficient also decreases, and the inlet wind temperature has little influence on the cooling wind temperature in this part. From the figure, it can be seen that the temperature of the cooling air in this part also basically does not change. Starting from −2 m is the exit section of the sintered ore; the cooling wind is basically not involved in heat exchange in this part, so the cooling wind temperature in this area is not affected by the inlet wind temperature, but this area is close to the inlet wind cap. So, with the increase in the inlet wind temperature, the temperature of the cooling wind in this area is also higher, but basically unchanged within the same working condition.

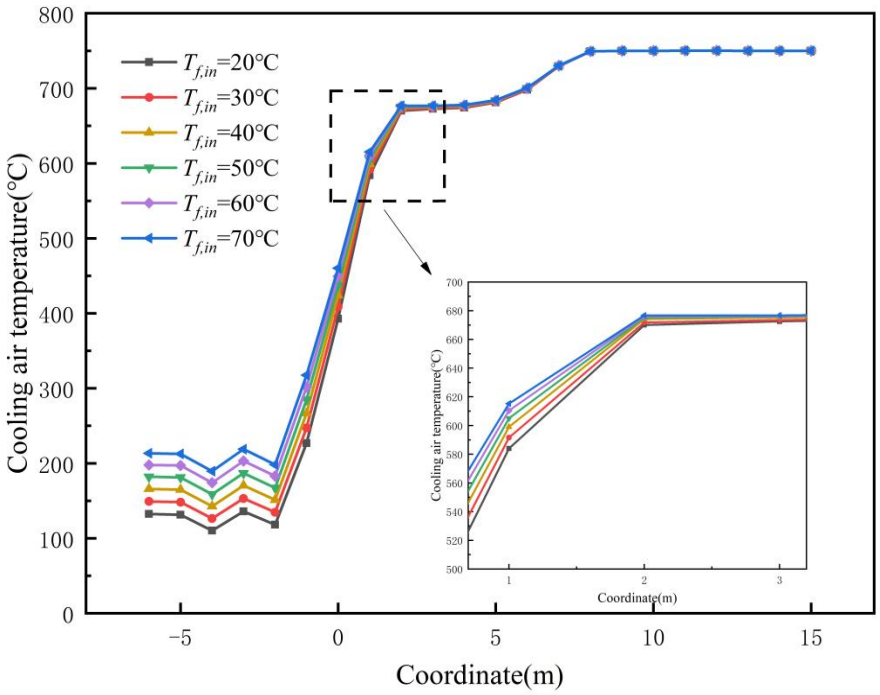

Figure 7. Cooling air temperature at different cooling air inlet temperatures axial variation diagram.

Figure 8 shows the radial variation in cooling air temperature under different cooling air inlet temperatures. In z = 1 m cross-section of the furnace cooling air temperature along the radial first increased and then decreased, showing the shape of the "M" type

distribution. The distribution of cooling air temperature along the radial direction at the same cross-section is not much affected by the working condition parameters, basically showing a low temperature in the central part of the chamber. The temperature on both sides of the air temperature rises, and the temperature of the cooling air immediately adjacent to the wall is decreasing. The reason is that the inlet air cap is cone-shaped, so the cooling wind enters the furnace through the cross duct, resulting in the centre part of the cooling wind temperature is small. And, with the cooling wind from the hood to the surrounding flow process and sintered ore cooling heat exchange, in the flow process of cooling, wind temperature increases and sintered ore is cooled. Near the wall, due to the wall effect, the cooling air temperature is slightly reduced at the wall.

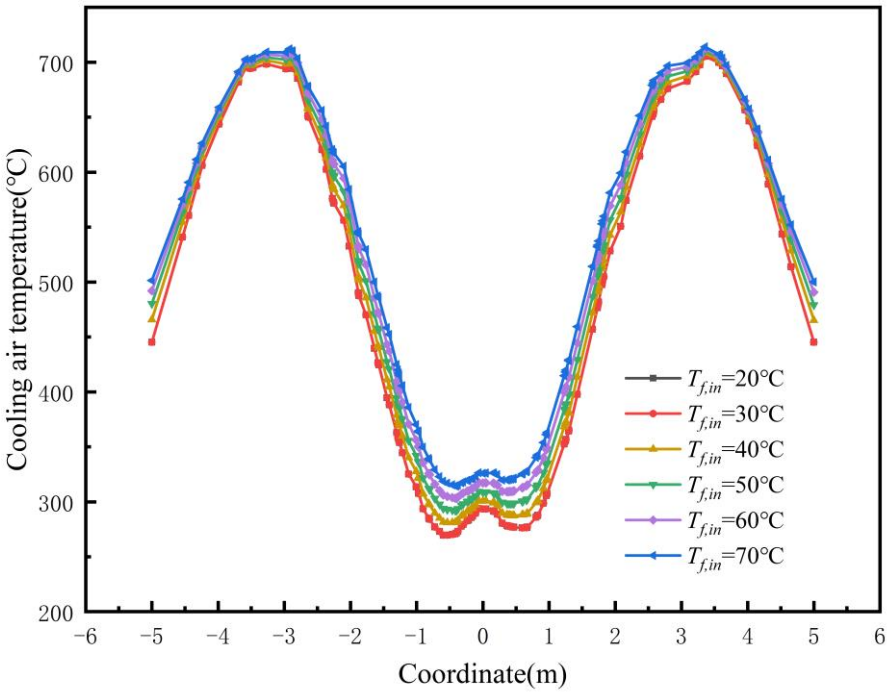

Figure 8. Radial variation in cooling air temperature for different cooling air inlet temperatures.

Table 3 shows the values of sintered ore and cooling air outlet parameters under different operating conditions, and the results are analysed below.

Table 3. Parameters of cooling air and sinter simulation results at different cooling air inlet temperatures.

Serial Number	Sinter Outlet Temperature (°C)	The Exergy Value of the Sintered Ore Outlet (kJ/kg)	Cooling Air Outlet Temperature (°C)	The Exergy Value of the Cooling Air Outlet (kJ/kg)
1	128.66	5408.46	692.81	31,809.14
2	145.16	6475.05	693.42	31,555.77
3	161.57	7555.36	694.89	31,429.27
4	177.51	8619.79	695.24	31,324.28
5	193.14	9675.43	695.48	31,161.58
6	208.44	10,718.44	695.64	31,169.59

Figure 9 shows the variation in cooling air and sinter outlet temperature for different sinter inlet air temperatures. When the inlet temperature of the sintered ore is 750 °C, the inlet velocity of the cooling air is 7.8 m/s, the height of the cooling section is 7 m, and the diameter of the cooling section is 10 m, the outlet temperatures of both the sintered ore and the cooling air increase with the increase in the inlet air temperature, and the increase in the outlet temperature of the sintered ore has a linear distribution, while the increase in the outlet temperature of the cooling air decreases gradually. The reason is that when the

cooling air inlet speed is unchanged, the influence of gas–solid heat transfer in the furnace is strengthened as the cooling air inlet temperature increases, so that the temperature at the cooling air outlet increases. Meanwhile, the sinter outlet temperature increases at the same rate as the cooling air inlet temperature increases.

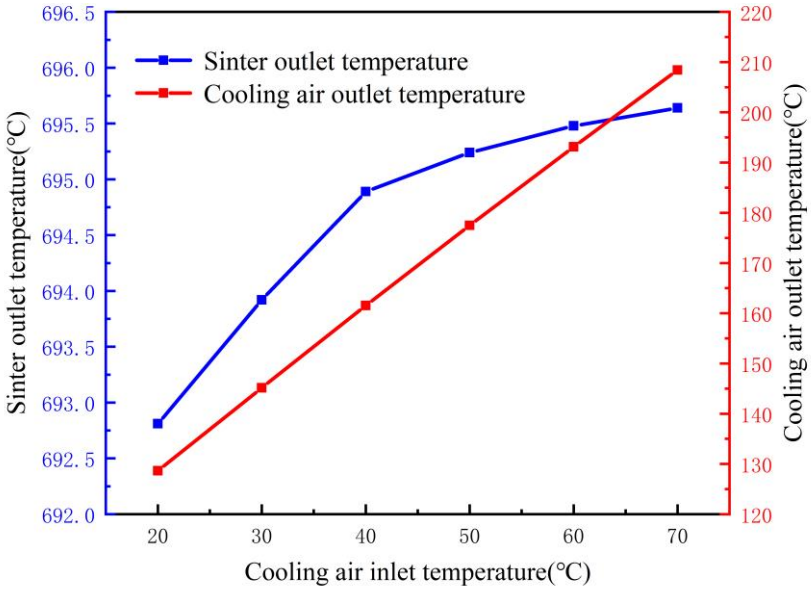

Figure 9. Variation in cooling air and sinter outlet temperature with cooling air inlet air temperature.

Figure 10 shows the increase in exergy and the variation in exergy efficiency of the cooling air in the cooling furnace for different cooling air inlet air temperatures. As the cooling wind inlet wind temperature increases, the temperature at the cooling wind outlet also increases, which results in a larger heat exchange between the wind and the mine. At the same time, the speed of the inlet cooling wind is constant, and the heat exchange effect in the furnace increases, resulting in the exergy carried by the cooling wind at the exit also increases. The exergy efficiency is affected by the increase in cooling wind exergy and sinter ore inlet exergy as shown in the formula. When the inlet temperature of the sintered ore is stable, the increase in the inlet air temperature leads to the increase in the exergy of the cooling air at the outlet, and then the exergy efficiency also increases.

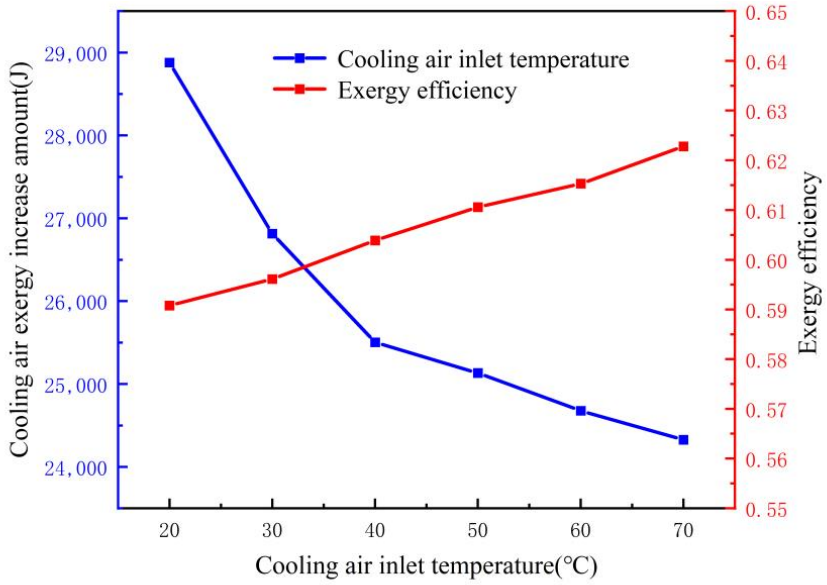

Figure 10. Variation in cooling air humidity value and efficiency with cooling air inlet air temperature.

3.2. Influence of Inlet Air Temperature on the Heat Exchange Effect of Vertical Sinter Ore Cooling Furnace

Numerical simulation of the heat transfer process in the furnace is carried out by changing the inlet ore temperature. The parameters of the inlet mine temperature are shown in Table 4, where the inlet air temperature is 20 °C, the height of the cooling section is 7 m, the diameter of the cooling section is 11.25 m, and the equivalent diameter of the sintered ore is 14.45 mm.

Table 4. Simulation parameters for inlet air temperature.

Scenario serial number	1	2	3	4	5	6
Imported ore temperature (°C)	600	680	760	840	920	1000

Figure 11 shows that with the increase in the sinter ore inlet temperature, the temperature of the sinter ore in the central section of the furnace gradually becomes larger. The reason is that with the increase in the inlet ore temperature, the cooling air and the hot sintered ore also undergo intense heat exchange, and the heat exchange effect is enhanced. However, the contact time between the sintered ore and the cooling air is constant due to the other parameters in the furnace remaining unchanged, which makes the sintered ore discharged before it is completely cooled. As a result, the temperature of the sinter in the central section of the furnace increases as the sinter inlet temperature increases. At the same time, as the sinter inlet temperature increases, the temperature of the sintered ore near the wall is lower and the temperature of the sintered ore in the furnace tends to be the same. This is because the higher temperature inlet sintered ore is not cooled to the same extent in the same time, so the temperature distribution in the furnace is not consistent.

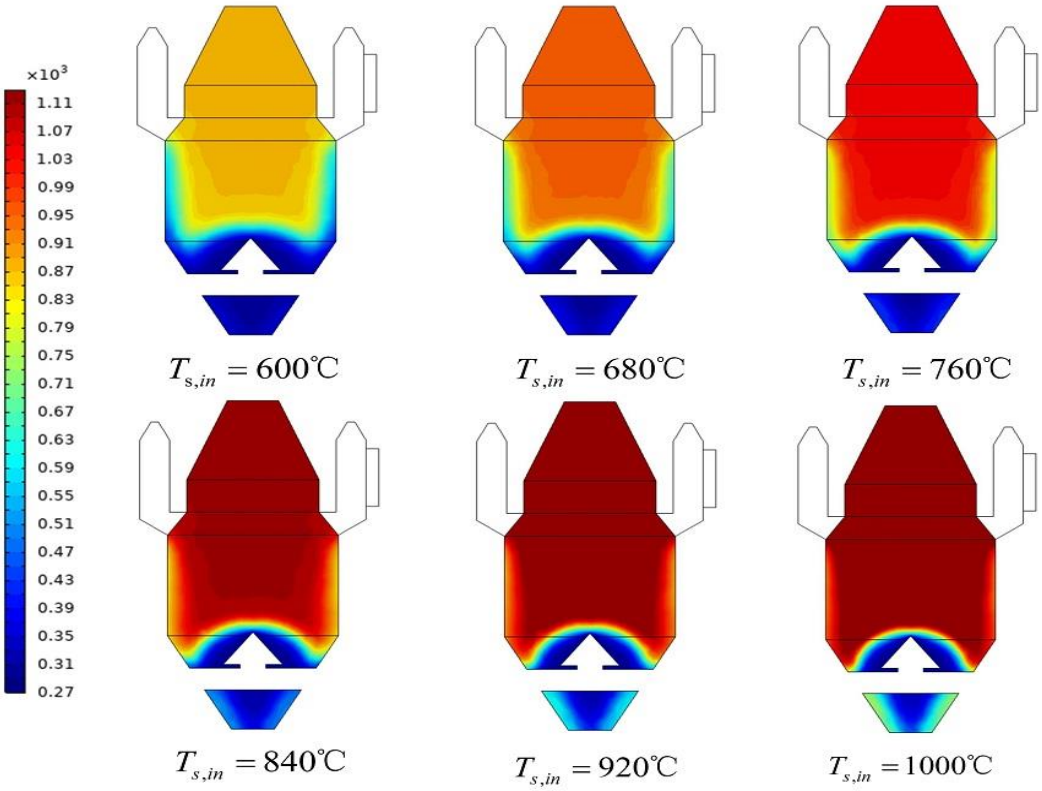

Figure 11. Variation in cooling air temperature with sinter inlet temperature at the central section of the furnace.

Figure 12 shows the variation in cooling air temperature with sinter ore inlet temperature at z = 3.5 m section in the furnace, and the following analyses are made. The

temperature of the sintered ore at the same height in the furnace increases gradually with the increase in the inlet temperature of the sintered ore. This is also because the high-temperature sintered ore is not sufficiently cooled in the furnace, and the higher the inlet temperature is, the heat exchange within the same cooling time is basically the same, so the overall temperature of the sintered ore in the furnace also increases. In addition, the temperature of the sintered ore near the wall is lower than the temperature of the sintered ore in the centre of the furnace.

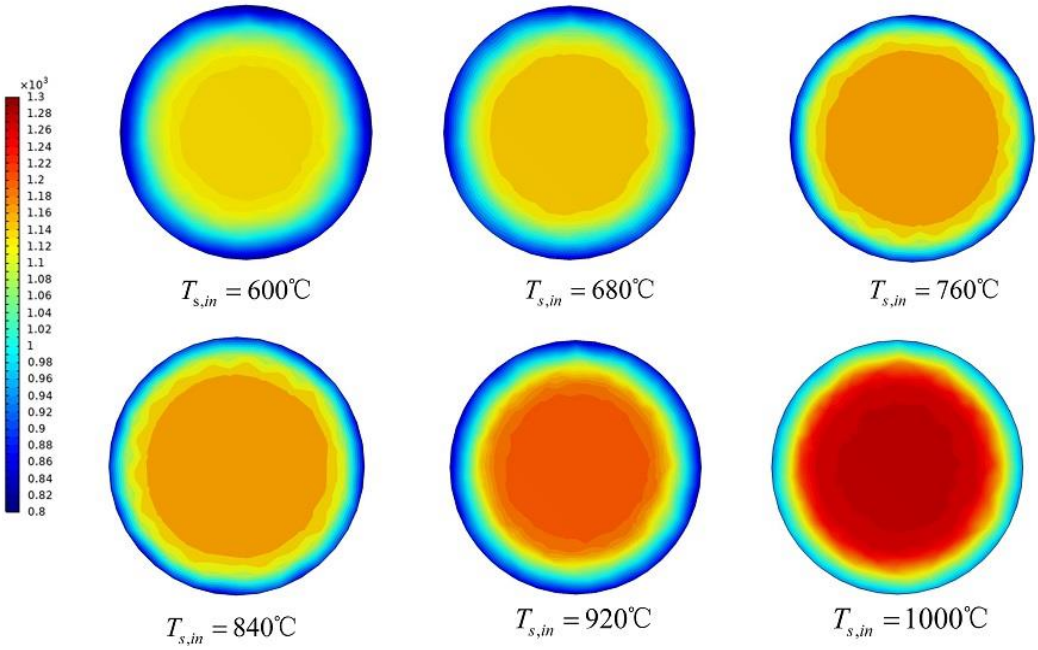

Figure 12. Variation in cooling air temperature with sinter inlet temperature.

Figure 13 shows the variation in sinter ore temperature along the axial direction in the furnace for different sinter ore inlet temperatures. With the increase in the sinter ore inlet temperature, the overall trend of the sinter ore temperature in the furnace increases, but the inlet ore temperature does not have much influence on the heat exchange process in the furnace. The temperatures of cooling air in the pre-storage section and sinter outlet section are basically unchanged under the same operating conditions. The reason is that the simulation process treats the high-temperature sinter as an isotropic porous medium, so when the inlet boundary value of the sinter temperature is changed, the overall heat transfer in the furnace is also enhanced with the increase in the inlet mine temperature, which makes the temperature of the cooling air at the same position also increase, but it remains unchanged under the same working condition.

Figure 14 shows the radial variation in sinter temperature at z = 1 m with different sinter inlet temperatures, and the following analyses are made. With the increase in sinter inlet temperature, the sinter in the furnace at the same height along the radial distribution of double "hump" type, basically flat at the cap, in the middle of the furnace diameter to reach the maximum, and near the wall and gradually decreased.

Table 5 shows the values of sinter and cooling air outlet parameters under different schemes.

Figure 15 shows the trend of cooling wind and sinter outlet temperature with the sinter inlet temperature. When the inlet temperature of the cooling air is 20 °C, the inlet air velocity of the cooling air is 7.8 m/s, the height of the cooling section and the diameter of the cooling section are 7 m and 10.0 m, respectively, the outlet temperatures of the cooling air and the sintered ore both increase with the increase in the sintered ore inlet temperature. The reason is that when the cooling wind flow rate is constant, the cooling time of the cooling wind on the sintered ore is also relatively constant. The sinter that is not

completely cooled within the same time is discharged, which increases the temperature of both the sinter and the cooling air at the outlet. In addition, the rate of increase in the outlet mine temperature becomes faster with the increase in the inlet mine temperature, while the rate of increase in the outlet temperature of the cooling air and the change in the inlet temperature of the sintered ore are basically the same, and both of them show a linear relationship.

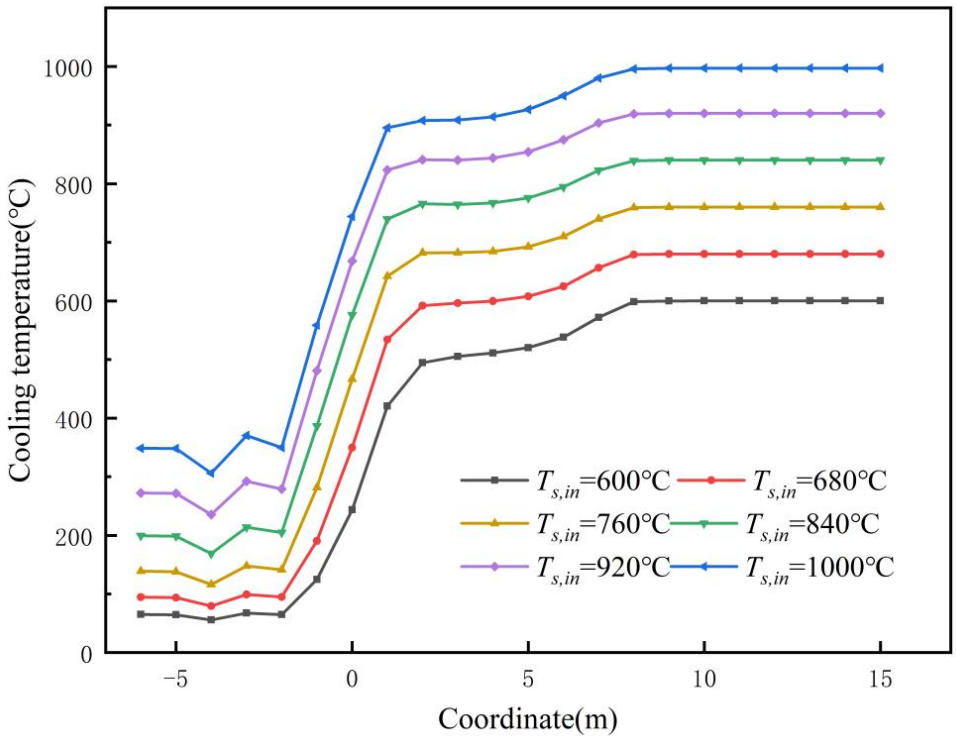

Figure 13. Sinter temperature variation along the axial direction at different sinter inlet temperatures.

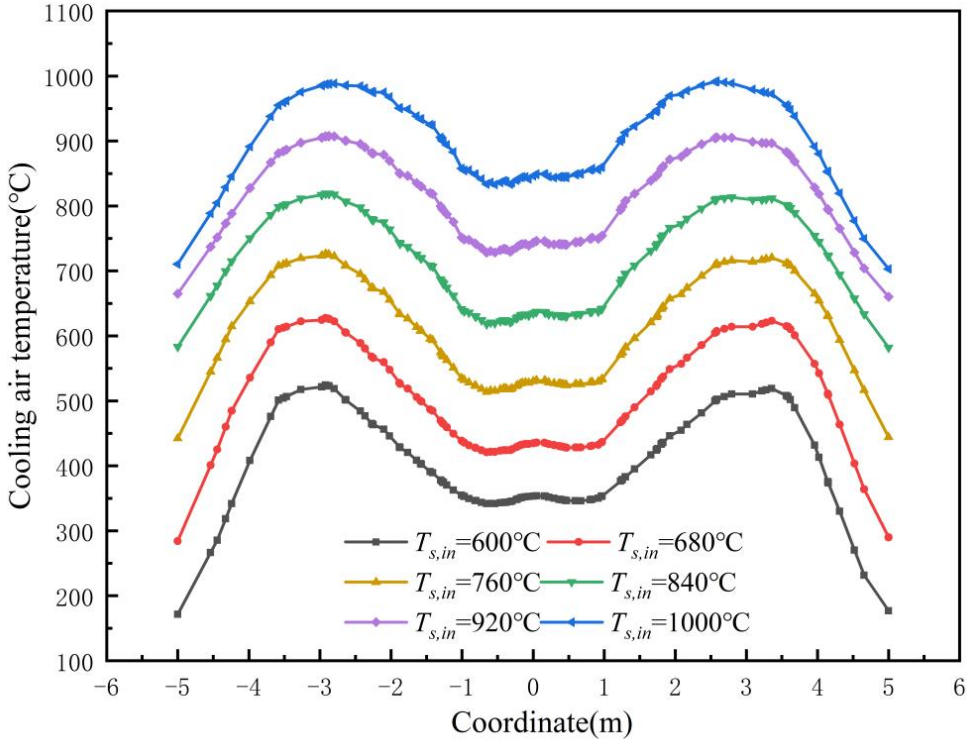

Figure 14. Sinter temperature variation along the radial direction for different sinter inlet temperatures.

Table 5. Parameters of cooling air and sinter simulation results at different sinter inlet temperatures.

Serial Number	Sinter Outlet Temperature (°C)	The Exergy Value of the Sintered Ore Outlet (kJ/kg)	Cooling Air Outlet Temperature (°C)	The Exergy Value of the Cooling Air Outlet (kJ/kg)
1	63.531	1545.69	523.29	23,147.11
2	91.984	3139.42	615.04	27,603.44
3	134.81	5803.41	703.39	31,858.97
4	193.19	9678.83	790.04	36,106.02
5	263.57	14,537.28	870.97	39,975.96
6	337.49	19,759.82	942.8	43,597.03

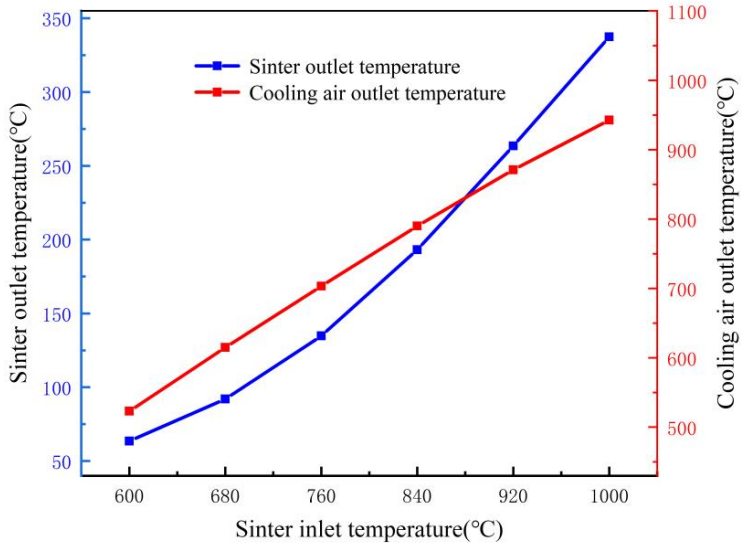

Figure 15. Variation in cooling air and sinter outlet temperature with inlet ore temperature.

Figure 16 shows the amount of exergy change and the change in energy efficiency of the cooling air in the furnace at different sinter ore inlet temperatures. Both the exergy increase and the energy efficiency of the cooling air in the furnace increase with the increase in the sinter inlet temperature, and basically show a linear distribution. The reason is that the cooling air outlet temperature increases linearly with the increase in sinter inlet temperature, and the exergy increases with the increase in sinter inlet temperature after the cooling air absorbs heat, and the increase is basically the same, as shown in the equation of exergy calculation.

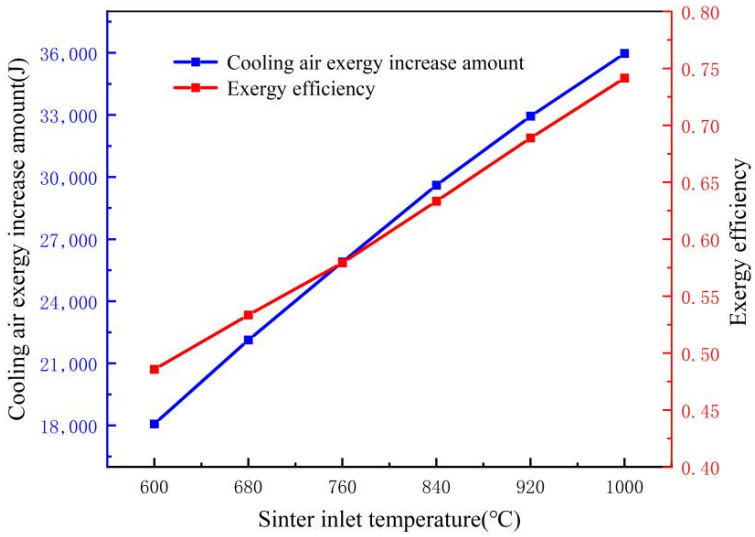

Figure 16. Variation in cooling air efficiency and efficiency with sinter inlet temperature.

3.3. Effect of Particle Equivalent Diameter on Gas–Solid Heat Transfer Characteristics

The heat transfer process in the furnace is numerically simulated by changing the sinter equivalent diameter. The parameters of the sinter equivalent diameter were selected as shown in Table 6, in which the inlet air temperature was 20 °C, the inlet ore temperature was 750 °C, the height of the cooling section was 7 m, and the diameter of the cooling section was 11.25 m.

Table 6. Simulation parameters for equivalent diameter.

Serial number	1	2	3	4	5	6
Equivalent diameter (mm)	6.05	10.30	14.45	18.80	23.05	27.30

Figure 17 illustrates the cooling air temperature distribution with sinter equivalent diameter in the centre profile of the shaft furnace. The sinter equivalent diameter has little influence on the overall heat transfer process in the furnace. The high-temperature sintered ore enters the furnace from the roof inlet and moves slowly from top to bottom, while the cooling air enters the furnace from the air cap and moves from bottom to top. In this process, the sintered ore moves to the cooling section and starts to be cooled, and the cooling wind absorbs heat and is gradually heated, and changing the equivalent diameter of the sintered ore in the process of gas–solid heat transfer does not have much effect on the heat transfer process in the furnace, so the trend of change in the figure is not obvious. The temperature of sintered ore in the centre part of the furnace tends to be the same, while the temperature near the wall decreases, because the sintered ore particles contact the wall of the cooling furnace, the hot sintered ore not only exchanges heat with the cooling air, but also exchanges heat with the wall at lower temperature, so the temperature of the sintered ore near the wall is lower.

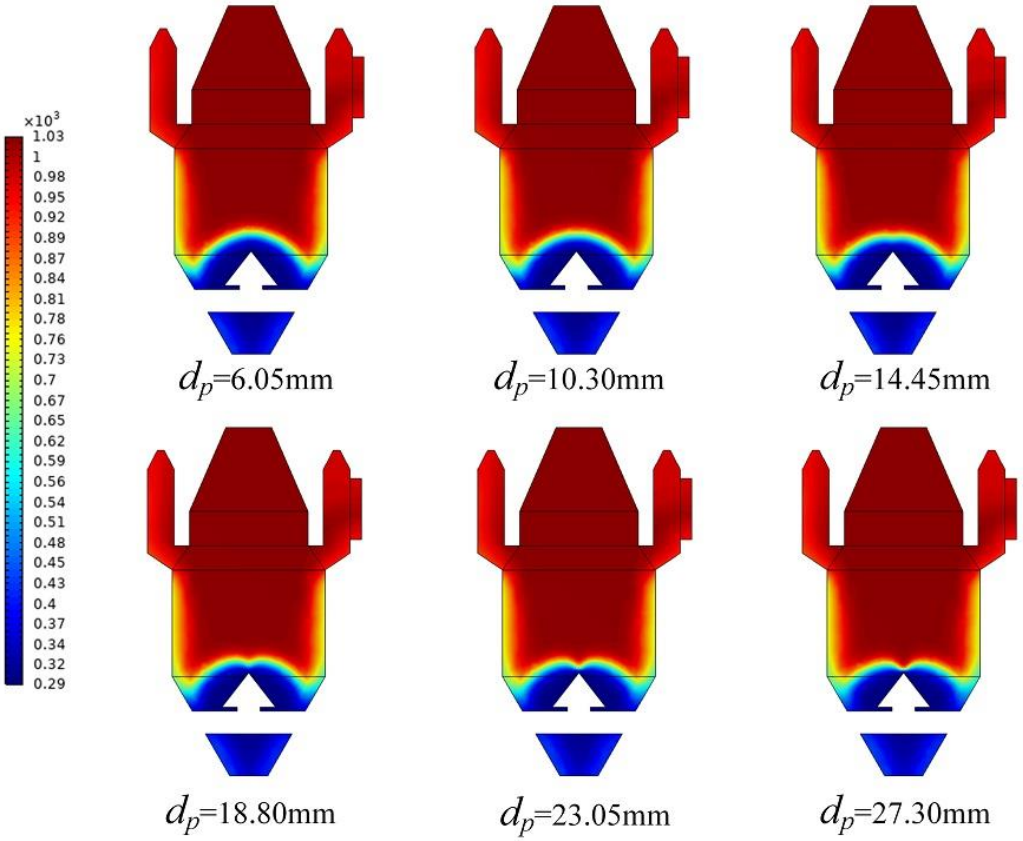

Figure 17. Variation in cooling air temperature with equivalent diameter at the central section of the furnace.

Figure 18 demonstrates the variation in cooling air temperature with equivalent diameter at the 3.5 m cross-section in the furnace. The cooling air temperature in the furnace does not change significantly at this cross-section, and the diameter of the sinter particles does not have much influence on the heat exchange process in the furnace. The temperature of the cooling air is the highest in the centre of the furnace, and gradually decreases along the radial direction to the surrounding area. The reason is that the cooling air along the radial flow to the surrounding process has been and hot sinter ore heat transfer, and basically in thermal equilibrium, the temperature and the sinter ore temperature is basically the same, the temperature is the lowest near the wall.

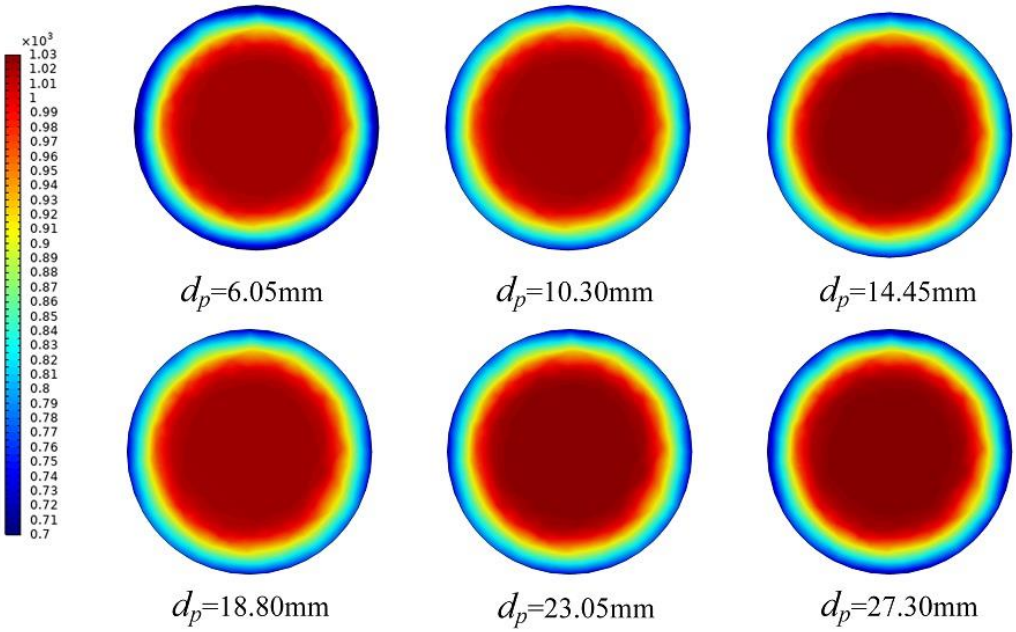

Figure 18. Variation in cooling air temperature with equivalent diameter.

Figure 19 shows the variation in cooling air temperature along the axial direction in the furnace for different sinter equivalent diameters, and the trend in the figure is analysed. With the increase in sinter equivalent diameter, the overall change in cooling air temperature in the furnace is not obvious, and the temperature of cooling air in the pre-storage section and sinter outlet section is basically unchanged under different working conditions. The reason is that the heat exchange effect in the furnace remains unchanged for a certain sinter inlet temperature and cooling air inlet temperature, which makes the effect of changing the sinter equivalent diameter on the temperature field in the furnace insignificant.

Figure 20 shows the radial variation in cooling air temperature with different equivalent diameters, and the trend is analysed in the figure. With the increase in the equivalent diameter of the sinter ore, the cooling air temperature in the cross-section along the radial direction of the middle of the low sides of the high class "M" type distribution. However, with the equivalent diameter from 18.80 mm to 27.30 mm, the temperature of the cooling air in the cooling furnace at the very centre of the cooling air is higher, because with the increase in the equivalent diameter of the sintered ore, the sintered ore and the cooling air at the part of the air cap heat transfer is the most intense, and at the same time, in the area nearer to the centre of the furnace, the lower the porosity of the sintered ore, the higher the flow rate of the cooling air, the convection in the region of the best heat transfer, so there is a higher temperature.

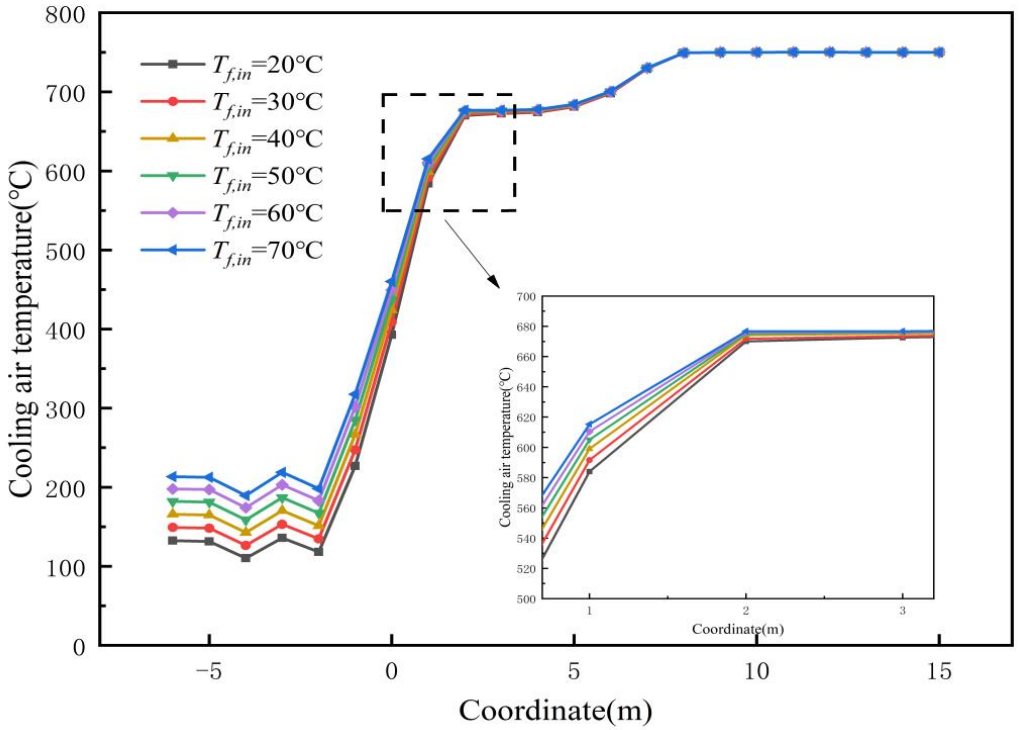

Figure 19. Axial variation in cooling air temperature at different equivalent diameters.

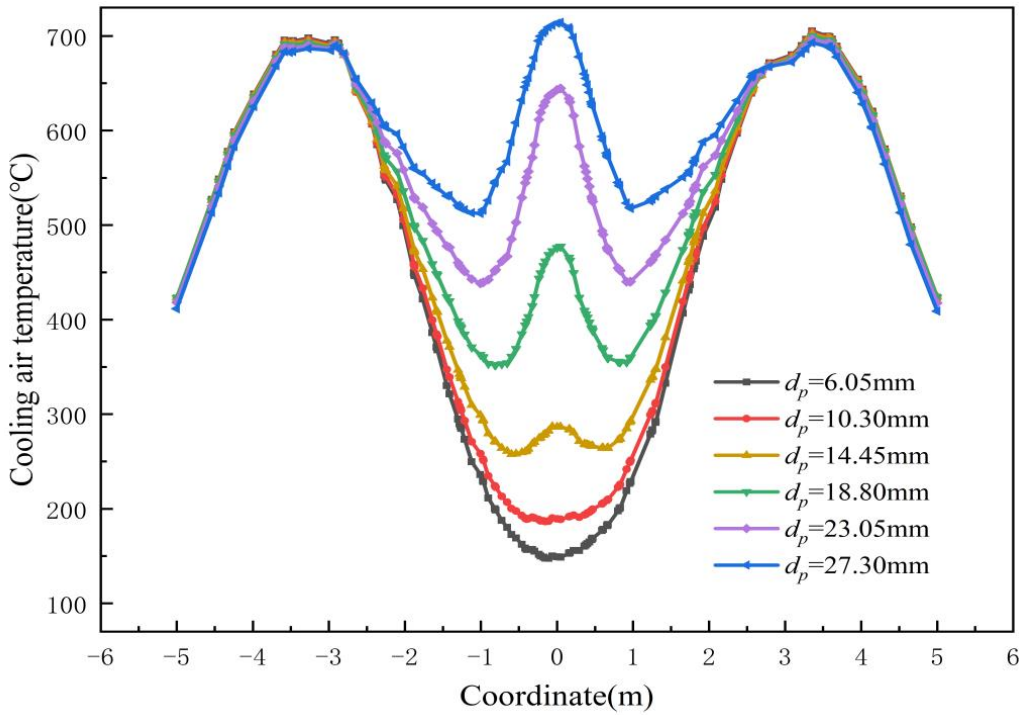

Figure 20. Variation in cooling air temperature in the radial direction for different equivalent diameters.

Table 7 shows the values of sinter and cooling air outlet parameters under different schemes.

Figure 21 demonstrates the variation in outlet cooling wind and sintered ore temperature with equivalent diameter. As can be seen from Figure 19, when the cooling air inlet temperature is 20 °C, the cooling air inlet wind speed is 7.8 m/s, the height of the cooling section and the diameter of the cooling section are 7 m and 10.0 m, respectively, the outlet wind temperature decreases with the increase in the equivalent diameter of the

sintered ore and the cooling air temperature decreases at a faster rate; the outlet mine temperature also increases with the increase in the equivalent diameter of the sintered ore and the magnitude of the increase in temperature becomes greater with the increase in the equivalent diameter of the sintered ore. Increases in the rate of temperature increase with the equivalent diameter of the sintered ore. This is because the expansion of the diameter of the sintered ore particles, the cooling air and sintered ore contact area becomes larger, resulting in a convective heat transfer coefficient with the expansion of the equivalent diameter of the particles, and as the gas–solid heat transfer becomes smaller, the export temperature of the ore rises and the export air temperature decreases.

Table 7. Parameters for cooling air and sinter simulation results at different equivalent diameters.

Serial Number	Sinter Outlet Temperature (°C)	The Exergy Value of the Sintered Ore Outlet (kJ/kg)	Cooling Air Outlet Temperature (°C)	The Exergy Value of the Cooling Air Outlet (kJ/kg)
1	128.71	5411.66	693.81	26,147.18
2	128.55	5401.43	692.88	26,108.42
3	128.66	5408.45	692.81	26,105.06
4	128.9	5423.46	692.55	26,094.11
5	129.11	5437.85	691.07	26,031.77
6	129.76	5478.86	689.37	25,960.18

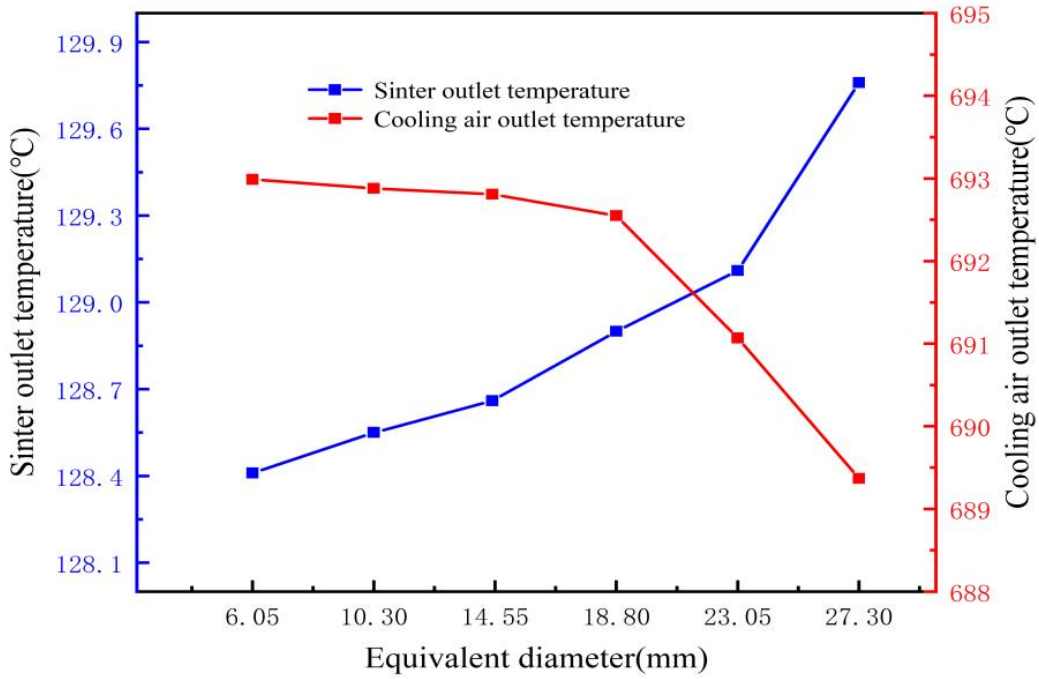

Figure 21. Variation in cooling air and sinter outlet temperature with equivalent diameter.

Figure 22 demonstrates the amount of exergy change and the change in exergy efficiency of the cooling air in the cooling furnace for different equivalent diameters. The increase in cooling air exergy decreases as the equivalent diameter increases. The reason is that the change in equivalent diameter of sintered ore makes the stacking density of particles change, and the larger the equivalent diameter is, the smaller the stacking density becomes, which makes the effect of heat exchange between the sintered ore and the cooling air increase. When the particle size decreases when the cooling air and sintered ore heat transfer is more gentle, the sintered ore heat transfer time is relatively longer, so is the equivalent diameter of the cooling air when the change in exergy is smaller, and expanding the equivalent diameter increases the cooling air exergy changes.

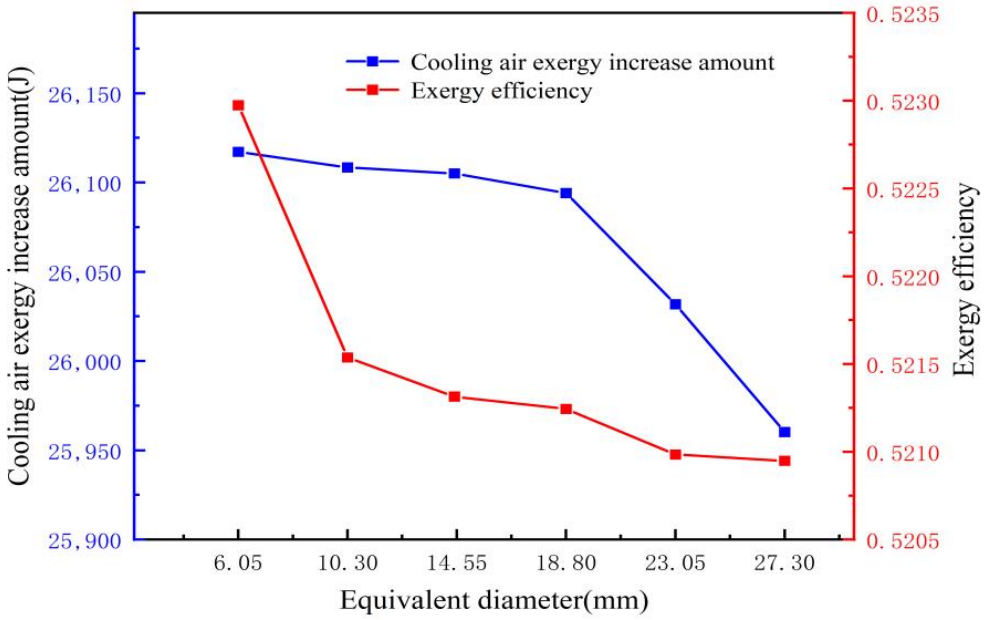

Figure 22. Variation in cooling air flow and efficiency with equivalent diameter.

3.4. Establishment of Gas–Solid Two-Phase Heat Transfer Correlation in a Furnace

In order to study the gas–solid heat transfer process in vertical cooling furnace, the dimensionality of heat transfer coefficient is analysed by the Π theorem.

According to the theoretical analysis, the factors affecting the heat transfer coefficient h in the furnace are air density, air flow rate u, diameter of sinter particles d, air viscosity μ, specific pressure heat capacity C_p, sinter thermal conductivity λ, etc., then there is the following relationship between the formula:

$$h = f(\rho, u, d, \mu, C_p, \lambda) \tag{11}$$

The seven variables mentioned above are all composed of the basic measures mass M, length L, time T and temperature Θ, so d, λ, μ, u are chosen as the basic measures, and the rest of the variables can be expressed by the four basic measures.

According to the Π theorem, the number of variables minus the number of basic measures is the number of Π-numbers, and three Π-numbers, Π_1, Π_2 and Π_3, can be obtained, then Equation (11) can be expressed as:

$$\Pi_1 = f\ (\ \Pi_2, \Pi_3) \tag{12}$$

The quantitative representation of all variables is shown in Table 8.

Table 8. Dimensions of variables.

The Variable Name	Symbol	Dimension
Heat transfer coefficient	h	$M\Theta^{-3}T^{-1}$
Air density	ρ	ML^{-1}
Air flow rate	u	$L\Theta^{-1}$
Particle diameter	d	L
Air viscosity	μ	$ML^{-1}\Theta^{-1}$
Specific constant pressure heat capacity	C_p	$ML^{-1}\Theta^{-1}$
Thermal conductivity	λ	$ML\Theta^{-2}T^{-1}$

(1) $\Pi_1 = d^a\lambda^b\mu^c u^d h = L^a\left(MLT^{-1}\Theta^{-3}\right)^b\left(ML^{-1}\Theta^{-1}\right)^c\left(L\Theta^{-1}\right)^d MT^{-1}\Theta^{-3}$

Then, the dimensionless form of Π_1 is:

$$\left.\begin{array}{l}\text{For mass dimensions M}: b+c+1=0\\ \text{For length dimensions } L: a+b-c+d=0\\ \text{For time dimensions } T: -b-c+d=0\\ \text{For temperature dimensions } \Theta: -3b-c-d-3=0\end{array}\right\}\text{Solution:} a=1, b=-1, c=0, d=0;$$

And then: $\Pi_1 = \frac{hd_p}{\lambda}$

$$(2)\ \Pi_2 = d^a\lambda^b\mu^c u^d\rho = \mathrm{L}^a\left(\mathrm{MLT}^{-1}\Theta^{-3}\right)^b\left(\mathrm{ML}^{-1}\Theta^{-1}\right)^c\left(\mathrm{L}\Theta^{-1}\right)^d\mathrm{ML}^{-3}$$

Then, the dimensionless form of Π_2 is:

$$\left.\begin{array}{l}\text{For mass dimensions M}: b+c+1=0\\ \text{For length dimensions } L: a+b-c+d-3=0\\ \text{For time dimensions } T: -b=0\\ \text{For temperature dimensions } \Theta: -3b-c-d=0\end{array}\right\}\text{Solution:} a=1, b=0, c=-1, d=1;$$

And then: $\Pi_2 = \frac{\rho u d_p}{\mu}$

$$(3)\ \Pi_2 = d^a\lambda^b\mu^c u^d c\mathrm{L}^a\left(\mathrm{MLT}^{-1}\Theta^{-3}\right)^b\left(\mathrm{ML}^{-1}\Theta^{-1}\right)^c\left(\mathrm{L}\Theta^{-1}\right)^d\mathrm{L}^{-2}\mathrm{T}^{-1}\Theta^{-2}$$

Then, the dimensionless form of Π_3 is:

$$\left.\begin{array}{l}\text{For mass dimensions M}: b+c=0\\ \text{For length dimensions } L: a+b-c+d+2=0\\ \text{For time dimensions } T: -b-1=0\\ \text{For temperature dimensions } \Theta: -3b-c-d-2=0\end{array}\right\}\text{Solution:} a=0, b=-1, c=-1, d=0;$$

And then: $\Pi_3 = \frac{\mu c}{\lambda}$

It can be known from fluid mechanics that $Nu = \frac{hd}{\lambda}$, $Re = \frac{\rho u d}{\mu}$, $Pr = \frac{\mu c}{\lambda}$, so $\Pi_1 = Nu$, $\Pi_2 = Re$, $\Pi_3 = Pr$; therefore, the following dimensionless equation is obtained:

$$Nu = f(Re, Pr) \tag{13}$$

The bed porosity is also a major factor affecting the heat exchange process between the sinter particles and the cooling air in the furnace as analysed in the previous section, so the dimensionless number is added to the equation of magnitude. In addition, the temperature difference between sinter and cooling air obtained from the simulation calculation exists in the cooling section in the region of more than 50 °C. At the same time, the cooling section is the most important gas–solid exchange process. At the same time, the cooling section is the most important gas–solid heat transfer area, so it is necessary to consider the change in the relevant physical properties in the heat transfer correlation equation, and it is not possible to distinguish the influence of the change in different physical properties on the heat transfer process only by the difference of the *Pr* number index. Therefore, a correction coefficient *Ct* [25] on temperature is introduced with the following expression:

$$C_t = \frac{T_f}{T_s} \tag{14}$$

Combining the above analyses, the following dimensionless equations can be obtained:

$$Nu = f(Re, Pr, \varepsilon, C_t) \tag{15}$$

By a process similar to the analysis of the bed pressure drop correlation equation, it can be seen that Equation (15) is also written in the form of a power function:

$$Nu = k\varepsilon^a Re^b Pr^c \left(\frac{T_f}{T_s}\right)^d \tag{16}$$

It can be shown that Equation (16) is the initial form of the correlation equation for the heat transfer of the flow within the bed of sintered ore particles obtained by using the method of magnitude analysis, where k, a, b, c, and d are coefficients to be determined.

The pending coefficients of the dimensionless equations were obtained from the data obtained from the design conditions using multiple regression analysis, and fitted based on Matlab 2022. The pending coefficients of the fitted equation are shown in Table 9.

Table 9. Results of fitting the empirical formula for the coefficients to be determined.

Coefficients to Be Determined	k	a	b	c	d
Fit the results	0.0466	−0.2	0.9582	0.4	0.0002

The empirical coefficients were substituted into the heat transfer correlation equation, which was fitted to obtain the correlation equation for heat transfer in the furnace:

$$Nu = 0.0466\varepsilon^{-0.2}Re^{0.9582}Pr^{0.4}\left(\frac{T_f}{T_s}\right)^{0.0002} \quad (17)$$

The conditions of use for this bed pressure drop correlation are as follows: $2300 \leq Re \leq 12700$, the range of cooling air inlet temperature is 20 °C~70 °C, the range of sinter inlet temperature is 600 °C~750 °C, the range of sinter equivalent diameter is 6.05 mm~27.30 mm, the range of bed porosity is 0.35~0.6, the range of height of cooling section is 6 m~8.5 m, and the range of bed diameter is 9 m~11.5 m.

Figure 23 shows the error analysis of the heat transfer correlation formula and the calculation results. As can be seen from Figure 23, the calculated results by the heat transfer correlation formula basically fall within the range of 30%, indicating that the calculation accuracy of this correlation formula is high, and the heat transfer correlation formula obtained by fitting is suitable for the prediction of the heat transfer effect in the furnace under this condition, which can provide an important reference for the subsequent research.

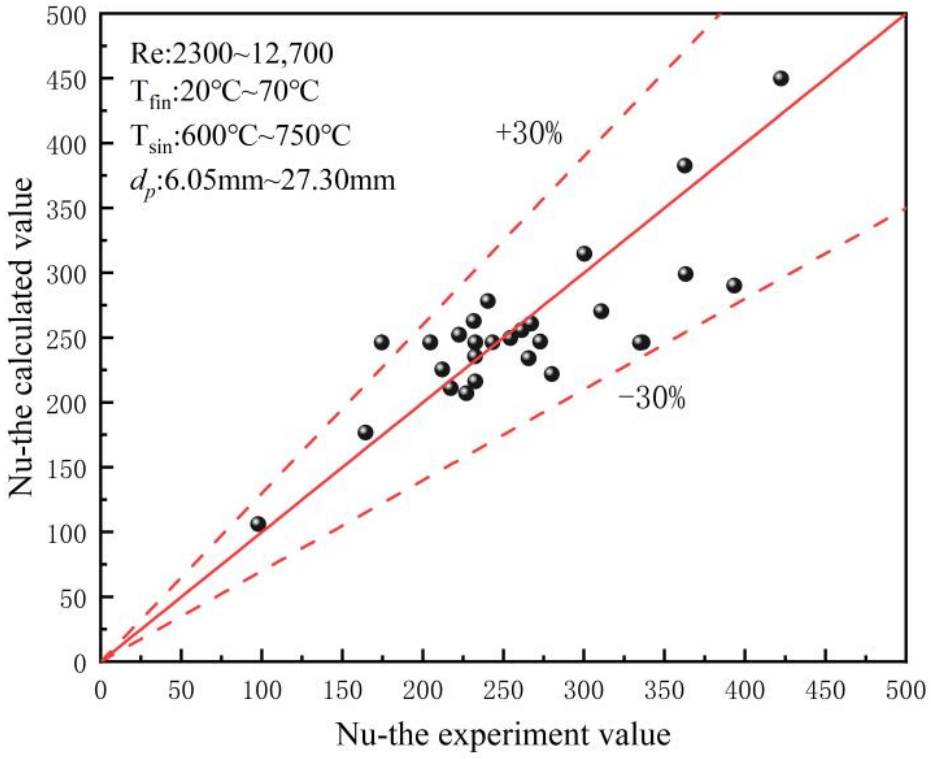

Figure 23. Heat transfer correlation versus test results.

4. Conclusions

Based on the established cooling furnace calculation model, the heat transfer mechanism of vertical sintering cooling furnace is studied. This paper mainly analysed the law of temperature distribution and heat transfer characteristics in sinter cooling furnace with different parameters, and adopt the concept of "exergy" to analyse the heat transfer effect in the cooling furnace. The specific conclusions are as follows:

- The cooling air inlet temperature and sinter ore inlet temperature are the main factors affecting the furnace temperature and gas–solid heat transfer characteristics, while other factors have less influence. The cooling air temperature in the furnace under each working condition shows a trend of low cooling air temperature in the middle, gradually increasing to the maximum value along the radial direction and then gradually decreasing. The cooling section is the most intense region of gas–solid heat exchange, and the temperature difference between the sintered ore and the cooling air in this section is the largest. The temperature of the cooling air in the pre-storage section and the sinter exit section is basically stable and does not change with the parameter changes.
- When the inlet air temperature increases, the outlet mine temperature increases, and the outlet mine temperature increases linearly, while the cooling air outlet temperature increases gradually. When the inlet mine temperature increases, both the outlet mine temperature and the outlet wind temperature increase, and the outlet mine temperature rise speed is gradually accelerated, but the outlet wind temperature rise speed is basically unchanged. When the sinter equivalent diameter increases, the outlet air temperature gradually decreases, and the decreasing speed gradually increases, while the outlet temperature gradually increases, and the increasing speed gradually increases. When the diameter and height of the cooling section increase, respectively, the outlet mine temperature decreases gradually, and the outlet air temperature decreases with the expansion of the cooling section diameter.
- Heat transfer correlations suitable for certain test conditions were obtained:

$$Nu = 0.0466\varepsilon^{-0.2}Re^{0.9582}Pr^{0.4}\left(\frac{T_f}{T_s}\right)^{0.0002}$$

The results of the calculations through the heat transfer correlation formula basically fall within the 30% range, and the accuracy of the calculations is high.

Author Contributions: Validation, R.L.; Investigation, B.T. and Y.R.; Writing—original draft, Q.W. and J.Z.; Writing—review & editing, W.X. and W.W.; Funding acquisition, Y.P. All authors have read and agreed to the published version of the manuscript.

Funding: This paper is supported by the Project of Central Plains Science and Technology Innovation Leading Talents of Henan Province (No. 224200510022).

Data Availability Statement: Data is contained within the article. The data presented in this study are available in all the charts and tables.

Conflicts of Interest: Author Juan Zhen was employed by the company Cscec Scimee Sci.& Tech. Co., Ltd., Author Yan Peng was employed by the company Citic Heavy Industries Co., Ltd., Louyang. The remaining authors declare that the research was conducted in the absence of any commercial or financial relationships that could be construed as a potential conflict of interest.

References

1. Xu, C.; Liu, Z.; Wang, S.; Liu, W. Numerical Simulation and Optimization of Waste Heat Recovery in a Sinter Vertical Tank. *Energies* **2019**, *12*, 385. [CrossRef]
2. Dong, H.; Zhao, Y.; Cai, J.; Zhou, W.; Ma, Y. Leakage of Sintering-Cooling System. *Iron and Steel* **2012**, *47*, 95–99. [CrossRef]
3. Dong, H.; Li, L.; Cai, J.; Liu, J.; Wang, B.; Suo, S. Process of Waste Heat Recovery and Utilization for Sinter in Vertical Tank. *China Metallurgy J.* **2012**, *22*, 6–11. [CrossRef]
4. Feng, H.; Chen, L.; Liu, X.; Xie, Z.; Sun, S. Constructal optimization of a sinter cooling process based on exergy output maximization. *Appl. Therm. Eng.* **2016**, *96*, 161–166. [CrossRef]

5. Feng, J.; Dong, H.; Zhao, Y. Numerical Investigation of Gas Flow in Vertical Tank for Recovering Sinter Waste Heat. *J. Northeast. Univ. (Nat. Sci. Ed.)* **2015**, *36*, 660–664. [CrossRef]
6. Feng, J.; Dong, H.; Gao, J.; Liu, J.; Liang, K. Theoretical and experimental investigation on vertical tank technology for sinter waste heat recovery. *J. Cent. South Univ.* **2017**, *24*, 2281–2287. [CrossRef]
7. Feng, J.; Dong, H.; Liu, J.; Gao, J.; Liang, K. Gas-solid heat transfer characteristics in vertical tank for sinter waste heat recovery. *J. Chem. Ind. Eng. (China)* **2015**, *66*, 4418–4423. [CrossRef]
8. Feng, J. Gas Solid Heat Transfer Process and Application Research in Vertical Tank for Sinter Waste Heat Recovery. Ph.D. Thesis, Northeastern University, Shenyang, China, 2017.
9. Feng, J.; Zhao, L.; Wang, H.; Cheng, Z.; Xia, Y.; Dong, H. Determination of Pressure Drop Correlation for Air Flow through Packed Bed of Sinter Particles in Terms of Euler Number. *Energies* **2022**, *15*, 4034. [CrossRef]
10. Tian, W.; Ni, B.; Jiang, C.; Wu, Z. Uncertainty analysis and optimization of sinter cooling process for waste heat recovery. *Appl. Therm. Eng.* **2019**, *150*, 111–120. [CrossRef]
11. Tian, W.; Jiang, C.; Ni, B.; Wu, Z.; Wang, Q.; Yang, L. Global sensitivity analysis and multi-objective optimization design of temperature field of sinter cooler based on energy value. *Appl. Therm. Eng.* **2018**, *143*, 759–766. [CrossRef]
12. Tian, F.; Huang, L.; Fan, L.; Qian, H.; Yu, Z. Wall effects on the pressure drop in packed beds of irregularly shaped sintered ore particles. *Powder Technol.* **2016**, *301*, 1284–1293. [CrossRef]
13. Fan, X.; Yang, H.; Tina, W.; Nie, A.; Hou, T.; Qiu, F.; Zhang, X. Catalytic Oxidation of chlorobenzene over MnOx/Al2O3-carbon Nanotubes Composites. *Catal. Lett.* **2011**, *141*, 158–162. [CrossRef]
14. Guo, Z.; Sun, Z.; Zhang, N.; Ding, M. Influence of confining wall on pressure drop and particle-to-fluid heat transfer in packed beds with small D/d ratios under high Reynolds number. *Chem. Eng. Sci.* **2019**, *209*, 115200. [CrossRef]
15. Gorman, J.M.; Zheng, A.; Sparrow, E.M. Bounding wall effects on fluid flow and pressure drop through packed beds of spheres. *Chem. Eng. J.* **2019**, *373*, 519–530. [CrossRef]
16. Mayerhofer, M.; Govaerts, J.; Parmentier, N.; Jeanmart, H.; Helsen, L. Experimental investigation of pressure drop in packed beds of irregular shaped wood particles. *Powder Technol.* **2011**, *205*, 30–35. [CrossRef]
17. Koekemoer, A.; Luckos, A. Effect of material type and particle size distribution on pressure drop in packed beds of large particles: Extending the Ergun equation. *Fuel* **2015**, *158*, 232–238. [CrossRef]
18. Park, J.H.; Lee, M.; Moriyama, K.; Kim, M.H.; Kim, E.; Park, H.S. Adequacy of effective diameter in predicting pressure gradients of air flow through packed beds with particle size distribution. *Ann. Nucl. Energy* **2018**, *112*, 769–778. [CrossRef]
19. Soma, J. Exergy transfer: A new field of energy endeavor. *Energy Eng.* **1985**, *82*, 11.
20. Dunbar, W.R.; Lior, N.R.; Gaggioli, A. Component equations of energy and exergy. *J. Energy Resour. Technol.* **1992**, *114*, 75. [CrossRef]
21. Cheng, Z.; Wang, H.; Feng, J.; Xia, Y.; Dong, H. Energy and Exergy Efficiency Analysis of Fluid Flow and Heat Transfer in Sinter Vertical Cooler. *Energies* **2021**, *14*, 4522. [CrossRef]
22. Prommas, R.; Rattanadecho, P.; Jindarat, W. Energy and exergy analyses in drying process of non-hygroscopic porous packed bed using a combined multi-feed microwave-convective air and continuous belt system. *Int. Commun. Heat Mass Transf.* **2012**, *39*, 242. [CrossRef]
23. Acevedo, L.; Uson, S.; Uche, J. Exergy transfer analysis of an aluminum holding furnace. *Energy Convers. Manag.* **2015**, *89*, 184. [CrossRef]
24. Zhang, S. Study on Flow and Heat Transfer Characteristics in the Sinter Vertical Cooling Process. Ph.D. Thesis, University of Science and Technology, Beijing, China, 2021.
25. Wang, M. Experimental Study on Heat Transfer Coefficient of Layer in Vertical Tank for Recovering Sinter Waste Heat. Master's Thesis, Northeastern University, Shenyang, China, 2012.